

Pressure control of the magnetic anisotropy of the quasi-2D van der Waals ferromagnet $\text{Cr}_2\text{Ge}_2\text{Te}_6$

T. Sakurai,^{1,*} B. Rubrecht,^{2,3,*} L. T. Corredor,^{2,*} R. Takehara,⁴ M. Yasutani,⁴ J. Zeisner,^{2,3}
A. Alfonsov,² S. Selzer,^{2,3} S. Aswartham,² A. U. B. Wolter,² B. Büchner,^{2,5} H. Ohta,⁶ and V. Kataev²

¹Research Facility Center for Science and Technology, Kobe University, Kobe 657-8501, Japan

²Leibniz IFW Dresden, D-01069 Dresden, Germany

³Institute for Solid State and Materials Physics, TU Dresden, D-01062 Dresden, Germany

⁴Graduate School of Science, Kobe University, Kobe 657-8501, Japan

⁵Institute for Solid State and Materials Physics and Würzburg-Dresden
Cluster of Excellence ct.qmat, TU Dresden, D-01062 Dresden, Germany

⁶Molecular Photoscience Research Center, Kobe University, Nada, Kobe 657-8501 Japan

(Dated: December 10, 2020)

We report the results of the pressure-dependent measurements of the static magnetization and of the ferromagnetic resonance (FMR) of $\text{Cr}_2\text{Ge}_2\text{Te}_6$ to address the properties of the ferromagnetic phase of this quasi-two-dimensional van der Waals magnet. The static magnetic data at hydrostatic pressures up to 3.4 GPa reveal a gradual suppression of ferromagnetism in terms of a reduction of the critical transition temperature, a broadening of the transition width and an increase of the field necessary to fully saturate the magnetization M_s . The value of $M_s \simeq 3\mu_B/\text{Cr}$ remains constant within the error bars up to a pressure of 2.8 GPa. The anisotropy of the FMR signal continuously diminishes in the studied hydrostatic pressure range up to 2.39 GPa suggesting a reduction of the easy-axis type magnetocrystalline anisotropy energy (MAE). A quantitative analysis of the FMR data gives evidence that up to this pressure the MAE constant K_U , although getting significantly smaller, still remains finite and positive, i.e. of the easy-axis type. Therefore, a recently discussed possibility of switching the sign of the magnetocrystalline anisotropy in $\text{Cr}_2\text{Ge}_2\text{Te}_6$ could only be expected at still higher pressures, if possible at all due to the observed weakening of the ferromagnetism under pressure. This circumstance may be of relevance for the design of strain-engineered functional heterostructures containing layers of $\text{Cr}_2\text{Ge}_2\text{Te}_6$.

Keywords: van der Waals magnet, 2D material, magnetic anisotropy, pressure effects, ferromagnetic resonance, magnetization

I. INTRODUCTION

The layered van der Waals magnet $\text{Cr}_2\text{Ge}_2\text{Te}_6$ [1] belongs to a class of materials which are currently the subject of intense research activities as these systems offer, on the one hand, a materials base for experimentally exploring details of two-dimensional magnetism [2–4]. On the other hand, the weak couplings between individual layers render these materials promising as (magnetic) components in so-called van der Waals heterostructures [5]. In both respects it is essential to properly characterize the magnetic anisotropies of the investigated materials. At zero external pressure, $\text{Cr}_2\text{Ge}_2\text{Te}_6$ features a uniaxial magnetic anisotropy with the magnetic easy axis being oriented parallel to the crystallographic c axis, i.e., perpendicular to the honeycomb layers extending in the ab plane (see, e.g., Refs. [1, 6–8]). In a previous study [9] we established the value of the uniaxial magnetocrystalline anisotropy energy density (MAE) $K_U = 0.48 \cdot 10^6 \text{ erg/cm}^3$ by means of ferromagnetic resonance (FMR) measurements under standard conditions at ambient pressure. A detailed discussion of this result and its comparison with the band structure calculations can be found in Ref. [9].

One route to modify the magnetic properties of van der Waals magnets is the application of hydrostatic pressure to the crystals, as, in the case of $\text{Cr}_2\text{Ge}_2\text{Te}_6$, was already attempted in Refs. [10, 11]. Z. Lin *et al.* [11] reported a change of the MAE upon applying external pressures up to 2 GPa, in particular a change of the sign of K_U . This implies that the anisotropy of the system transforms from *easy-axis type* (easy axis parallel to the crystallographic c axis) to *easy-plane type* (easy direction perpendicular to the c axis and, thus, in the ab plane). However, details of the MAE as a function of applied pressure have not been investigated so far. This motivates a systematic, combined magnetization and FMR study on $\text{Cr}_2\text{Ge}_2\text{Te}_6$ at various hydrostatic pressures aiming at a quantification of the pressure dependence of K_U . To our knowledge, the FMR experiments on $\text{Cr}_2\text{Ge}_2\text{Te}_6$ under pressure and the magnetization studies at pressures exceeding 1 GPa were not reported so far.

In the present work we communicate a comprehensive investigation of the effect of the hydrostatic pressure on the static magnetic and FMR properties of single crystals of $\text{Cr}_2\text{Ge}_2\text{Te}_6$ at pressures up to $P = 2.39$ and 3.4 GPa applied in the FMR and magnetization experiments, respectively. With increasing pressure, the magnetic ordering temperature gradually decreases from $T_c = 66$ K at $P = 0$ down to 45 K at $P = 3.4$ GPa. Concomitantly, the transition width broadens and the saturation field in-

* These authors contributed equally to this work.

creases. Remarkably, the saturation magnetization stays practically constant up to $P = 2.8$ GPa and decreases at a higher pressure. The FMR measurements performed at $T = 4.2$ K $\ll T_c$ in a frequency range 50–260 GHz for the two orientations of the applied magnetic field $\mathbf{H} \parallel c$ and $\mathbf{H} \perp c$ evidence that the excitation energy gap characteristic of an easy-axis ferromagnet closes at $P > 2$ GPa. The data analysis in the frame of a phenomenological theory of FMR reveals that the seemingly isotropic magnetism of the studied crystals manifesting in the gap closure is a result of the compensation of the intrinsic easy-axis magnetocrystalline anisotropy of $\text{Cr}_2\text{Ge}_2\text{Te}_6$ and the shape anisotropy of the sample. It follows from our analysis that the MAE constant K_U is reduced by a factor of 2 at the highest applied pressure in the FMR experiment but still remains sizable. This suggests a robustness of the easy-axis-type of ferromagnetism of $\text{Cr}_2\text{Ge}_2\text{Te}_6$ to the application of pressure up to $P = 2.39$ GPa despite a reduction of T_c . Our findings motivate further pressure experiments to address the question if the sign of the MAE could be changed at still high pressures before the ferromagnetic state would be fully suppressed. From the technological perspective, the results of the present work on the pressure-tunability of the magnetic anisotropy of $\text{Cr}_2\text{Ge}_2\text{Te}_6$ may be insightful for accessing the use of this material as a magnetic element of spintronic devices with the strained architecture.

II. SAMPLES AND METHODS

Single crystals of $\text{Cr}_2\text{Ge}_2\text{Te}_6$ were grown with the self flux technique and thoroughly characterized as described in detail in our previous work in Ref. [9]. As grown single crystals were thoroughly characterized by powder x-ray diffraction and energy dispersive x-ray spectroscopy, both agree well with the crystal structure in the R3 space group as well as with the expected stoichiometry of $\text{Cr}_2\text{Ge}_2\text{Te}_6$ [12].

The bulk magnetization data were measured using a custom-built pressure cell for a commercial Quantum Design superconducting quantum interference device (SQUID) magnetometer (MPMS-XL). Inside the CuBe cell, two opposing cone-shaped ceramic anvils compress a CuBe gasket with a cylindrical hole used as sample chamber [13, 14]. The platelet-like shaped single-crystalline sample ($m = 3.3 \times 10^{-6}$ g) of $\text{Cr}_2\text{Ge}_2\text{Te}_6$ with the c axis normal to the plate was installed into the gasket hole (diameter $\varnothing = 0.6$ mm and height $h = 0.8$ mm) and rested on the flat part of the ceramic anvil. Given the longitudinal magnetic field direction in the SQUID magnetometer the $\mathbf{H} \parallel c$ orientation was easily achieved. The uniaxial force is applied at ambient temperature, and it is converted into hydrostatic pressure in the sample chamber using Daphne oil 7575 as pressure-transmitting medium. We checked the pressure value and its homogeneity at low temperature by measuring the pressure dependent diamagnetic response associated with the super-

conducting transition of a small Pb manometer inserted in the sample space [15]. Such measurements were performed in applied fields of $H = 5$ Oe. In order to ensure a stable pressure throughout all measurements due to the thermal expansion of the cell upon temperature sweeps, a thermal cycling was performed once from ambient temperature to 2 K and back to ambient temperature before the actual data acquisition.

Note, that a magnetic background is detected in our DC magnetization measurements arising from the pressure cell itself. Here, we performed a detailed magnetic characterization of the empty pressure cell within the same conditions of the real experiments for the aim of a quantitative and reliable disentanglement of the sample signal from the overall magnetic response. The background correction was done by subtracting the fitted signal of a gasket without a sample measured under the same conditions, given that the raw signal of the gasket in our setup can be described by a magnetic dipole in our SQUID detection coils. While at temperatures above ~ 20 K a temperature-independent pressure cell background ensures an excellent background subtraction, at low temperatures a strongly temperature dependent magnetization of the CuBe cell limits the resolution of our experiments. Consequently, only background subtracted data for $T > 10$ K are shown. Small kinks in the magnetization curves around 40 K were identified as instrumental artifacts. More detailed information about the background of our pressure cell can be found in Ref. [16]. Still, the combination of the very small magnetization above the ferromagnetic ordering temperature of our samples with a very small mass ($m \sim 3.3 \times 10^{-6}$ g) and the large uncertainty of absolute pressure values for $T > 150$ K using Pb as a manometer at low T in our ceramic anvil pressure cell restrains us from a quantitative Curie-Weiss analysis in the high-temperature regime.

Ferromagnetic resonance is a resonance response of the total magnetization of the ferromagnetically ordered material exposed to the microwave radiation. The FMR frequency is determined not only by the strength of the applied external magnetic field but also sensitively depends on the magnetic anisotropy of the studied sample, as will be explained in Sect. III B. The magnetic anisotropy can be accurately quantified by measuring FMR at different excitation frequencies. Therefore, in the present work FMR experiments were carried out using a multi-frequency electron spin resonance setup equipped with a piston-cylinder pressure cell with a maximum pressure of about 2.5 GPa. Its detailed description can be found in Ref. [17]. Microwave radiation with frequencies in a range 50 – 260 GHz was provided by a set of Gunn-diode oscillators and detected by a ^4He -liquid cooled hot-electron InSb bolometer. Magnetic fields up to 10 T were generated by a cryogen-free superconducting magnet. Platelet-like single-crystalline samples of $\text{Cr}_2\text{Ge}_2\text{Te}_6$ with the typical lateral dimensions of $\sim 3 - 4$ mm were put inside the pressure cell in a Teflon capsule filled with a pressure-transmitting fluid (Daphne 7373 oil from

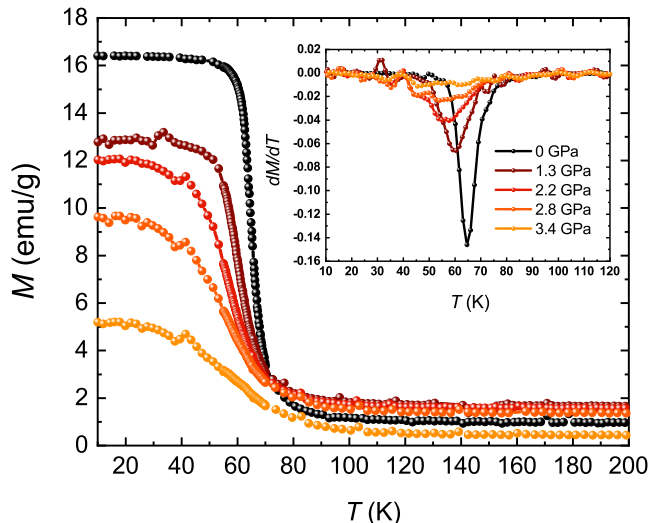


FIG. 1. Temperature dependence of the magnetization $M(T)$ of $\text{Cr}_2\text{Ge}_2\text{Te}_6$ measured in the FC mode at $\mu_0 H = 0.1$ T parallel to the c axis for pressures up to 3.4 GPa. The inset shows the corresponding $dM(T)/dT$ curves.

Idemitsu Kosan Co., Ltd [18–20]). The advantage of having a well-defined c axis direction of the samples facilitated their orientation in the FMR pressure cell. For the $\mathbf{H} \parallel \mathbf{c}$ field geometry the studied sample was placed on the flat bottom of the Teflon capsule. For $\mathbf{H} \perp \mathbf{c}$ it was firmly fixed with a thin Teflon tape to the side of a small rectangular parallelepiped placed on the bottom of the Teflon capsule. The inner pistons of the pressure cell made of ZrO_2 -based ceramics ensured a low-loss propagation of the microwaves through the cell. The pressure was calibrated using a superconducting tin-based pressure gauge. All FMR measurements were performed at a temperature $T = 4.2$ K for two orientations of the sample with respect to the applied magnetic field, $\mathbf{H} \parallel \mathbf{c}$ axis and $\mathbf{H} \perp \mathbf{c}$ axis, respectively.

III. EXPERIMENTAL RESULTS AND DISCUSSION

A. Pressure-dependent magnetization study

The field-cooled (FC) magnetization curves $M(T)$ as a function of temperature are shown in Fig. 1 for an applied magnetic field $\mu_0 H = 0.1$ T oriented parallel to the c axis under an applied pressure up to 3.4 GPa. Due to the small magnetization values, resulting from the very small mass of the sample, the absolute values at high temperature show an artificial shift in the magnetization axis, coming from a highly sensitive background subtraction. Two main characteristics are observed. First, the onset of the magnetic transition at approximately 80 K is persistent within ± 1 K despite the pressure change. The

onset was determined from the derivative dM/dT curve (Fig. 1, inset) while moving from high to low temperature as the point of its departure from a very small, close to zero value $dM/dT \sim 0$ caused by just a small polarization of paramagnetic moments to the negative values due the gradual development of the spontaneous ferromagnetic moment. Second, the transition broadens continuously, and the ferromagnetic (FM) transition temperature T_c , defined as the minimum of the $dM(T)/dT$ curve [21, 22], shifts to lower temperature upon increasing pressure, as shown in the inset of Fig. 1. This behavior is in line with an earlier report [10] where magnetization measurements at pressures up to 1 GPa showed the same tendency. Remarkably, the absolute value of the magnetization in the FM state at the given field of the measurement is gradually reduced with increasing the pressure up to 3.4 GPa. This can be explained by a shift of the saturation field H_{sat} as function of pressure to higher values, which reduces consequently the magnetization at small applied fields such as 0.1 T (see Fig. 2 and discussion below).

The magnetic field dependence of the magnetization $M(H)$ is depicted in Fig. 2 for the same pressure values as shown for the temperature dependences. To minimize the influence of the non-perfect subtraction of the background signal from the pressure cell at low temperatures, the curves were measured at $T = 15$ K, which is still low enough to capture the characteristic behavior of the FM state (cf. Fig. 1). The $M(H)$ data set in Fig. 2 includes a reference measurement performed at ambient pressure on a more massive single crystal ($m \sim 4$ mg) and without the pressure cell. The ambient pressure data yield a saturation moment M_s of $3.05 \mu_B/\text{Cr}$, which is consistent with the value found in our previous study [9]. Importantly, the data in Fig. 2 show that M_s is pressure independent up to about 2.8 GPa within the experimental error bar, the latter mostly being determined by the comparably strong background signal due to the reduced mass of our sample. At higher pressure, however, M_s reduces to about $2.5 \mu_B/\text{Cr}$ at 3.4 GPa. Another important observation is that, contrary to the saturation moment, the saturation field H_{sat} continuously shifts to higher values under applied hydrostatic pressure. While saturation can be achieved at ~ 0.1 T for ambient pressure, $\mu_0 H_{\text{sat}}$ increases to ~ 1.5 T at 3.4 GPa. A possible explanation for the shift of the saturation field has been proposed by Sun *et al.* [10] through first principles calculations. According to them, the pressure-induced decrease in the Cr-Cr bond length favors antiferromagnetic (AFM) exchange, while a concomitant deviation from the 90° Cr-Te-Cr bond angle leads to a suppression of the FM superexchange interaction. An increasing competition between the easy-axis MAE and the easy-plane shape anisotropy under pressure (see below) may also contribute to an increase of H_{sat} . Magnetization measurements at still higher pressures would be enlightening in this regard.

The results of the above analysis of the $M(T)$ and $M(H)$ dependences are summarized in Fig. 3, where we plot the M_s and T_c values as a function of the ap-

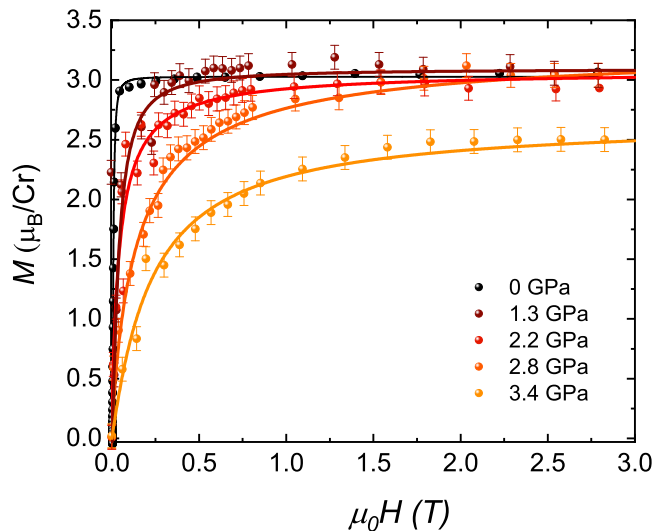


FIG. 2. Magnetization M as a function of applied field $\mathbf{H} \parallel c$ at $T = 15$ K for pressures up to 3.4 GPa. The solid lines are guides to the eye. A demagnetization correction has been applied [23].

plied pressure with the corresponding experimental error bars. As already noticed above, the ordering temperature value estimated from the first derivative criterion is less accurate for higher pressures due to the broadening of the transition under pressure (Fig. 1, inset). Still, we could clearly validate the long-range ordered ferromagnetic ground state of $\text{Cr}_2\text{Ge}_2\text{Te}_6$ at 4.2 K and up to 3.4 GPa, i.e., for the parameter ranges where FMR experiments were performed (see below). In contrast to T_c , the FM saturation moment is approximately constant for pressures up to 2.8 GPa with a subsequent reduction for $P > 2.8$ GPa.

B. Pressure-dependent FMR study

The FMR data sets presented in this section were collected by measuring three different single-crystalline samples of $\text{Cr}_2\text{Ge}_2\text{Te}_6$ from the same batch with similar, but slightly different, lateral dimensions. As will be discussed below, the differences in demagnetization factors associated with different sample dimensions are, however, negligible in the analysis of the FMR data.

Selected FMR spectra measured for the two field geometries used in this work are shown in Figs. 4(a) and (b). A shift of the signal to higher fields for $\mathbf{H} \parallel c$ and to smaller fields for $\mathbf{H} \perp c$, respectively, by applying pressure is clearly visible. The results of frequency-dependent FMR measurements at a temperature of 4.2 K with $\mathbf{H} \parallel c$ and at different applied external pressure between 0 and 2.39 GPa are summarized in Fig. 4(c). At 0 GPa, $\text{Cr}_2\text{Ge}_2\text{Te}_6$ features an easy-axis type MAE with the easy axis oriented parallel to the c axis as has been investigated in detail in our previous study [9]. This kind

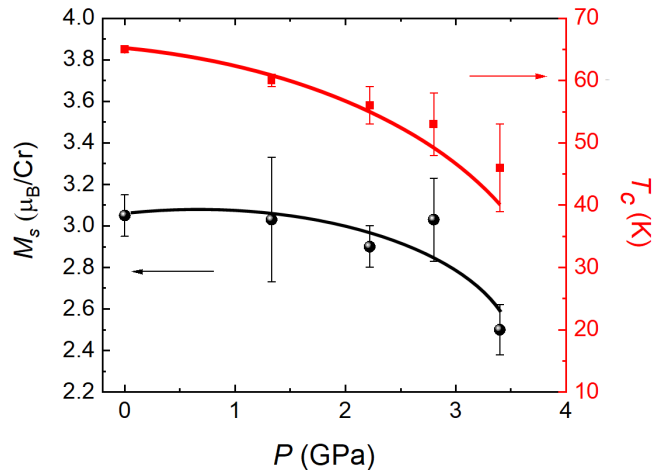


FIG. 3. Saturation magnetization M_s and the FM transition temperature T_c as a function of the applied pressure (symbols). M_s was calculated as the average magnetization value for applied fields $\mu_0H \geq 2$ T, which was determined as the lower limit of the applied field at which $dM/dH = 0$ for all the curves within the experimental error bar. The solid lines are guides to the eye.

of anisotropy directly manifests in an FMR measurement by a shift of the resonance line towards smaller magnetic fields with respect to the resonance position in the paramagnetic state if the external magnetic field \mathbf{H} is applied parallel to the magnetic easy axis (c axis) and towards higher magnetic fields if \mathbf{H} is normal to the magnetic easy axis. This behavior is illustrated in Figs. 4(a) and (b) where, depending on the direction of the applied field, the FMR signal at $P = 0$ is shifted either to the left or to the right side of the signal from the paramagnetic reference sample 2,2-diphenyl-1-picrylhydrazyl (DPPH) with a g factor $g \simeq 2$ which is commonly used as a magnetic field marker. Remarkably, the application of an external pressure counteracts these tendencies by shifting the FMR line towards the paramagnetic position for both field geometries. As a result, with increasing the applied pressure from $P = 0$ to 2.01 GPa the FMR signal from the sample becomes isotropic, i.e., the resonance field H_{res} does not depend on the direction of the applied field at this value of pressure [Fig. 5(b)].

The frequency-field dependence of the paramagnetic reference sample DPPH is shown in Fig. 4 as a blue dashed line for comparison with the ferromagnetic resonance fields H_{res} measured on the $\text{Cr}_2\text{Ge}_2\text{Te}_6$ samples for $\mathbf{H} \parallel c$ axis. H_{res} shifts continuously to higher magnetic fields with increasing P and thereby approach, but do not cross, the paramagnetic resonance branch in the frequency-field diagram. This systematic shift is emphasized in the inset of Fig. 4 where details of the frequency-field diagram are shown for intermediate field strengths. The change of the FMR line position as a function of external pressure evidences a reduction of the MAE of the studied system. However, the shift of the resonance fields

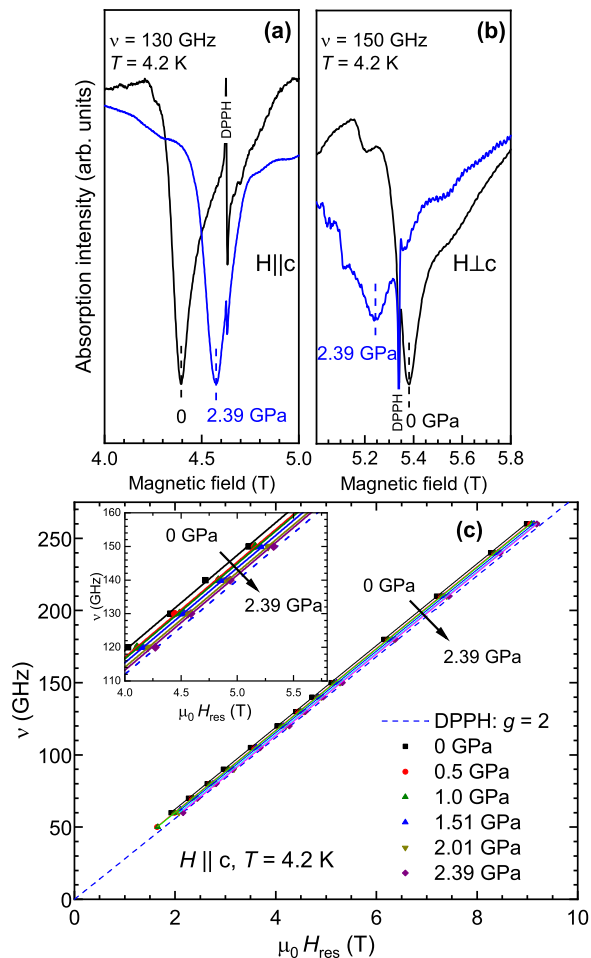


FIG. 4. Representative FMR spectra of $\text{Cr}_2\text{Ge}_2\text{Te}_6$ at zero and the maximum applied pressure for the applied magnetic field parallel (a) and perpendicular (b) to the c -axis. The sharp spike is a signal from the paramagnetic reference DPPH with a g factor of $g \simeq 2$. Some distortions of the lineshape can be ascribed to the interference effects of the microwaves in the pressure cell [24, 25]; (c) The frequency-field diagram obtained from FMR measurements at various pressures up to 2.39 GPa for $\mathbf{H} \parallel c$. Solid lines are fits according to Eq. (2) while the dashed blue line indicates the paramagnetic $\nu(H_{\text{res}})$ dependence of the DPPH reference sample with $g \simeq 2$. Details of the frequency-field diagram for intermediate fields are shown in the inset in order to emphasize the systematic shift of the resonance line with increasing pressure.

of $\text{Cr}_2\text{Ge}_2\text{Te}_6$ is not only determined by the strength and the sign of the MAE constant K_{U} but also by demagnetization fields resulting from the specific sample shapes which favor, in the case of the plate-like shaped $\text{Cr}_2\text{Ge}_2\text{Te}_6$ crystals, an in-plane magnetization. As a consequence, the internal demagnetization fields will lead to a shift of the resonance position to higher fields if the external magnetic field is applied perpendicular to the honeycomb layers, i.e., for $\mathbf{H} \parallel c$ axis. Thus, the size of the anisotropy constant K_{U} derived from shifts of the resonance position would be underestimated, if demagne-

tization effects are not taken into account (cf. the related discussion in Ref. [9]). These demagnetization fields H_{D} can be calculated using the elements of the demagnetization tensor N_i ($i = x, y, z$, with x, y, z being the principal axes of the tensor) [23, 26, 27]:

$$H_{\text{D}}^i = -4\pi N_i M \quad , \quad (1)$$

where M denotes the magnetization of the sample. Since the thickness of the plate-like samples used in this study could not be quantified precisely, the real sample shape was approximated using the demagnetization factors for a flat (infinite) plate oriented perpendicular to the z axis (which was chosen to coincide with the crystallographic c axis of $\text{Cr}_2\text{Ge}_2\text{Te}_6$), i.e., $N_x = N_y = 0$, $N_z = 1$. This assumption is supported by the fact that the lateral dimensions in the ab plane of the used $\text{Cr}_2\text{Ge}_2\text{Te}_6$ crystals were much larger than the thicknesses of the samples parallel to the c axis. Using the value of the saturation magnetization $M_{\text{s}} \simeq 3 \mu_{\text{B}}/\text{Cr}$ (which corresponds to $M_{\text{s}} \approx 201 \text{ erg/G cm}^3$ for $\text{Cr}_2\text{Ge}_2\text{Te}_6$) yields a demagnetization field $\mu_0 H_{\text{D}}$ in the fully saturated ferromagnetic phase of -0.253 T if the external field is applied parallel to the c axis. The frequency-field dependences measured with this field orientation were then fitted by the following expression

$$\nu_{\text{res}} = \frac{g\mu_{\text{B}}\mu_0}{h} [H_{\text{res}} + H_{\text{D}} + H_{\text{A}}] \quad , \quad (2)$$

where ν_{res} denotes the resonance/microwave frequency and H_{A} is the anisotropy field describing the intrinsic magnetocrystalline anisotropy. Fits of Eq. (2) to the measured data are shown in Fig. 4(c) as solid lines. For the fitting, the g factor as well as H_{A} were treated as free fit parameters. The g -factor varied very little within the error bars around the mean value of 2.03 (see, Sect. IV) whereas H_{A} was significantly decreasing with increasing the pressure. Using the latter parameter it is possible to calculate the uniaxial MAE K_{U} according to (see, for instance, Ref. [28])

$$K_{\text{U}}^{\text{fit}} = \frac{H_{\text{A}} M_{\text{s}}}{2} \quad . \quad (3)$$

The results obtained from this fitting procedure are discussed in the following section together with results from an alternative approach for a quantitative analysis of the FMR data.

IV. SIMULATIONS OF THE FREQUENCY DEPENDENCE AND DETERMINATION OF THE MAGNETIC ANISOTROPIES

In order to simultaneously take into account the results of our FMR measurements performed with $\mathbf{H} \parallel c$ and $\mathbf{H} \perp c$ field geometries, the measured frequency-field dependences were numerically simulated for each pressure value. This lead to a refinement of the determination of

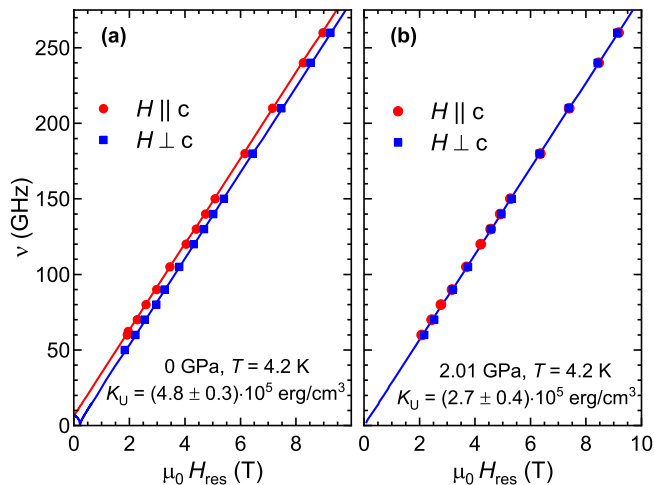


FIG. 5. Examples for simulations (solid lines) of the measured frequency-field dependences (symbols) at (a) 0 GPa and (b) 2.01 GPa, respectively. In these simulations experimental data sets obtained for $\mathbf{H} \parallel c$ (circles) and $\mathbf{H} \perp c$ (squares) were taken into account simultaneously in order to determine the value of K_U .

K_U , in particular at higher pressures. For the simulations we used a well established phenomenological model of FMR (see, e.g., Refs. [28–30]) where the resonance frequency ν_{res} is expressed as

$$\nu_{res}^2 = \frac{g^2 \mu_B^2}{h^2 M_s^2 \sin^2 \theta} \left(\frac{\partial^2 F}{\partial \theta^2} \frac{\partial^2 F}{\partial \varphi^2} - \left(\frac{\partial^2 F}{\partial \theta \partial \varphi} \right)^2 \right). \quad (4)$$

Here, F is the free energy density, and θ and φ are the spherical coordinates of the magnetization vector $\mathbf{M}(M_s, \varphi, \theta)$.

This phenomenological model is applicable for ferromagnets with the fully saturated magnetization at temperatures sufficiently lower than T_c , i.e., in the case of the fully developed ferromagnetic phase. According to the above discussed results of our pressure-dependent magnetization study both criteria are safely fulfilled for the T , P and H parameter ranges of the FMR study.

To obtain the resonance position of the FMR signal, F in Eq. (4) should be taken at the equilibrium angles φ_0 and θ_0 of \mathbf{M} . In the simulations, the minimum of F with respect to θ and φ for a given set of experimental parameters, such as the microwave frequency and the direction and the strength of the magnetic field, was found numerically. For $\text{Cr}_2\text{Ge}_2\text{Te}_6$, an account of both an intrinsic uniaxial magnetic anisotropy and of (extrinsic) shape anisotropy of the particular studied sample enabled an accurate description of all FMR data sets. In this case the free energy density (in cgs units) is defined as

$$F = -\mathbf{H} \cdot \mathbf{M} - K_U \cos^2(\theta) + 2\pi M_s^2 (N_x \sin^2(\theta) \cos^2(\varphi) + N_y \sin^2(\theta) \sin^2(\varphi) + N_z \cos^2(\theta)) \quad (5)$$

and comprises, besides the Zeeman energy density expressed by the first term, contributions due to the uniaxial and shape anisotropies, second and third terms, respectively.

Representative simulations of frequency-dependent measurements at 0 and 2.01 GPa are shown in Figs. 5(a) and (b), respectively. At 0 GPa, the separation of the $\nu(H_{res})$ curves obtained for the two different field orientations clearly evidences the easy-axis type magnetic anisotropy with the $\mathbf{H} \parallel c$ curve being shifted to smaller fields and the $\mathbf{H} \perp c$ curve being shifted to higher fields as compared to the paramagnetic position, respectively. The 0 GPa data could be simulated using the value for K_U of $4.8 \cdot 10^5 \text{ erg/cm}^3$ obtained in our previous study [9]. Keeping the value of K_U fixed, the g factor as well as demagnetization factors were adjusted in order to consistently describe different studied samples. It turned out that all 0 GPa data could be described successfully with an isotropic g factor of 2.03, which is consistent with our previous investigations, and the same set of demagnetization factors $N_x = N_y = 0$, $N_z = 1$ despite the (small) differences in the shapes of the samples. These parameters were kept fixed in the simulations of the frequency dependences measured at several non-zero pressures. The only free parameter in these simulations was the anisotropy constant K_U which allowed to determine the pressure dependence of the MAE. As can be seen in Fig. 5(b), at a pressure of 2.01 GPa, the measured frequency dependences are nearly identical for both orientations of the external magnetic field (a similar frequency-field diagram was obtained for 2.39 GPa), giving the impression of an isotropic behavior. However, the contributions of the magnetocrystalline anisotropy and the shape anisotropy to the free energy density [Eq. (5)] have opposite sign within the pressure range of this study. Thus, the apparently isotropic frequency dependence is, in fact, a consequence of the similar strength of these two contributions. This allows to conclude that an application of pressures between 2.01 and 2.39 GPa reduces the uniaxial MAE K_U to a value that compensates the shape anisotropy of the crystals. With the demagnetization field $\mu_0 H_D = -0.253 \text{ T}$ and the saturation magnetization $M_s \approx 201 \text{ erg/G cm}^3$ estimated above one obtains the shape anisotropy constant $K_{shape} = (H_D M_s)/2 \approx -2.54 \cdot 10^5 \text{ erg/cm}^3$. Its absolute value is indicated by the dashed line in Fig. 6. Moreover, the pressure-dependent FMR studies do not provide any evidence for a pressure-induced sign change of the magnetocrystalline anisotropy or a vanishing of the intrinsic uniaxial anisotropy up to pressures of 2.39 GPa. This is in contrast to the conclusions drawn in Ref. [11] on a spin reorientation transition at pressures between 1.0 and 1.5 GPa based on magneto-transport investigations of $\text{Cr}_2\text{Ge}_2\text{Te}_6$.

The pressure dependence of K_U as obtained from fitting of the $\mathbf{H} \parallel c$ data to Eq. (2) and from the simulations of all data available for both field orientations according to Eq. (5) is shown in Fig. 6. Qualitatively, both methods reveal a similar behavior, in particular a reduction of K_U

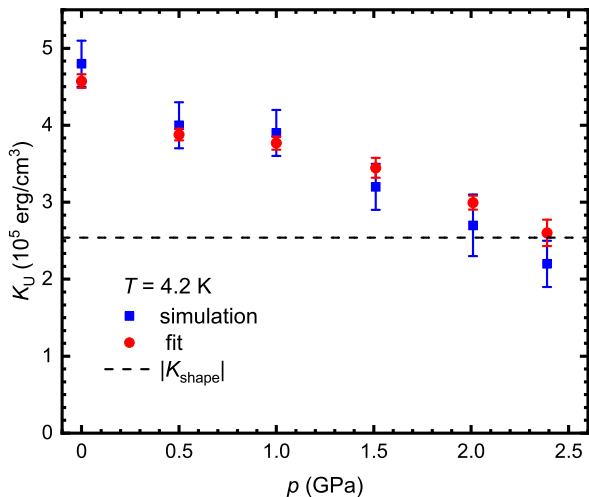


FIG. 6. Pressure dependence of the uniaxial magnetocrystalline anisotropy constant K_U of $\text{Cr}_2\text{Ge}_2\text{Te}_6$. Red circles denote the results obtained from fitting the different $\nu(H_{\text{res}})$ curves according to Eq. (2) for $\mathbf{H} \parallel c$. Blue squares are the K_U values determined from simulations according to Eq. (5) considering the experimental data sets for $\mathbf{H} \parallel c$ and $\mathbf{H} \perp c$ simultaneously. The horizontal dashed line shows the absolute value of the negative shape anisotropy constant $K_{\text{shape}} \approx -2.54 \cdot 10^5$ erg/cm 3 . It compensates the decreasing positive value of K_U at $p \gtrsim 2$ GPa yielding a seemingly isotropic behavior.

with increasing pressure. However, the deviation between the K_U values derived from the fits and the simulation increases at higher pressures. This could be attributed to the fact that the simulations simultaneously take into account the frequency dependences measured for both field orientations. Therefore, the reliability of the K_U values from simulations is higher despite the larger error bars, in particular at higher pressures at which differences between both field orientations become very small. Finally, it is worthwhile mentioning that in Ref. [31] a pressure-induced difference in the unit-cell volume of $\text{Cr}_2\text{Ge}_2\text{Te}_6$ between applied pressures of 0 and 3 GPa of about 4% was reported. As the unit-cell volume enters into the calculation of the saturation magnetization, such a reduction of volume with increasing pressure could change the absolute value determined for K_U . However, it was found that the pressure-induced contraction of the unit-cell volume by 4% does not affect the determination of K_U but is within the given error bars.

V. CONCLUSIONS AND OUTLOOK

Our combined magnetization and ferromagnetic resonance study on single crystals of the quasi-two-dimensional ferromagnet $\text{Cr}_2\text{Ge}_2\text{Te}_6$ has revealed a significant effect of the application of hydrostatic pressure P on the properties of the ferromagnetic state of this compound. It manifests in a reduction of the critical temper-

ature T_c and a concomitant broadening of the transition to the FM state, as well as in a gradual increase of the saturation field H_{sat} . In contrast, the saturation magnetization remains practically constant up to $P = 2.8$ GPa and reduces by approaching the highest applied pressure of 3.4 GPa. The frequency dependent FMR measurements performed in a fully developed FM state at $T \ll T_c$ and $H > H_{\text{sat}}$ at various external pressures up to 2.39 GPa revealed a systematic shift of the resonance fields with increasing P evidencing a continuous reduction of the magnetocrystalline anisotropy constant K_U . From the quantitative analysis of the data, which takes into account demagnetization effects, it follows that K_U , although being significantly reduced at highest pressures applied in this study, neither vanishes nor changes its sign up to pressures of about 2.4 GPa. Therefore, noting that FMR is a very direct method for the quantitative determination of magnetic anisotropy, it can be concluded with confidence that there is no evidence for a switching of the magnetic anisotropy from the easy-axis to the easy-plane type within the pressure range under consideration. Further pressure dependent studies of $\text{Cr}_2\text{Ge}_2\text{Te}_6$ are appealing to understand the apparent discrepancy between our work and the magneto-transport study in Ref. [11] claiming a spin-reorientation transition in $\text{Cr}_2\text{Ge}_2\text{Te}_6$ at pressures 1 GPa $< P < 1.5$ GPa, and to address the question whether a pressure-induced sign-switching of the magnetic anisotropy could be achieved at pressures exceeding 2.39 GPa.

Although in terms of the spatial dimensionality we investigated bulk, 3-dimensional crystals of $\text{Cr}_2\text{Ge}_2\text{Te}_6$, we showed in our previous ESR/FMR study that the low-temperature magnetism of the bulk crystals is essentially of a 2D nature due to a very weak interlayer magnetic coupling in this van der Waals compound [9]. Considering this intrinsic magnetic two-dimensionality of the bulk material our pressure dependent study can be relevant for the research on $\text{Cr}_2\text{Ge}_2\text{Te}_6$ in the truly 2D spatial limit. In this respect, the pressure control of the magnetic anisotropy investigated in our work may provide important hints for a targeted design of functional magneto-electrical heterostructures containing layers of $\text{Cr}_2\text{Ge}_2\text{Te}_6$.

In particular, a recent prediction of a remarkable strain and electric field tunability of a single layer $\text{Cr}_2\text{Ge}_2\text{Te}_6$ is encouraging [32]. It remains yet an open question regarding the design of a heterostructure where the strain ϵ of the order $\pm(1-2)\%$ for the $\text{Cr}_2\text{Ge}_2\text{Te}_6$ layer, as proposed in Ref. [32], can be achieved. However, a sizable effect on the magnetic anisotropy which we observed at pressures up to 2.39 GPa corresponds to an even smaller compressive in-plane strain $\epsilon \sim 0.7\%$ [31]. Such straining seems to be plausible to achieve since, in general, 2D van der Waals materials are known to sustain large strain. For example, it was shown that the biaxial compressive and tensile strain of $\sim 1\%$ can be achieved in the single layer molybdenum dichalcogenide deposited on a thermally compressed or expanded polymer substrate [33].

ACKNOWLEDGMENTS

The work in Kobe was partially supported by Grants-in-Aid for Scientific Research (C) (No. 19K03746) from Japan Society for the Promotion of Science.

The work in Dresden was supported by the Deutsche Forschungsgemeinschaft (DFG) through Grant KA1694/12-1 and within the Collaborative Research Center SFB 1143 “Correlated Magnetism – From Frustration to Topology” (project-id 247310070) and the Dresden-Würzburg Cluster of Excellence (EXC 2147) “ct.qmat - Complexity and Topology in Quantum Matter” (project-id 39085490). S.A. acknowledges financial support by the DFG through Grant AS 523/4-1. A.A. acknowledges financial support by the DFG through Grant No. AL 1771/4-1. S.S. acknowledges financial support from GRK-1621 Graduate Academy. V.K. gratefully acknowledges hospitality and financial support during his research visit at Kobe University.

-
- ¹ V Carteaux, D Brunet, G Ouvrard, and G Andre, “Crystallographic, magnetic and electronic structures of a new layered ferromagnetic compound $\text{Cr}_2\text{Ge}_2\text{Te}_6$,” *J. Phys.: Condens. Matter* **7**, 69 (1995).
- ² J.-G. Park, “Opportunities and challenges of 2D magnetic van der Waals materials: magnetic graphene?” *J. Phys.: Condens. Matter* **28**, 301001 (2016).
- ³ Cheng Gong, Lin Li, Zhenglun Li, Huiwen Ji, Alex Stern, Yang Xia, Ting Cao, Wei Bao, Chenzhe Wang, Yuan Wang, Z. Q. Qiu, R. J. Cava, Steven G. Louie, Jing Xia, and Xiang Zhang, “Discovery of intrinsic ferromagnetism in two-dimensional van der Waals crystals,” *Nature* **546**, 265 (2017).
- ⁴ Kenneth S. Burch, David Mandrus, and Je-Geun Park, “Magnetism in two-dimensional van der Waals materials,” *Nature* **563**, 47 (2018).
- ⁵ M. Gibertini, M. Koperski, A. F. Morpurgo, and K. S. Novoselov, “Magnetic 2D materials and heterostructures,” *Nat. Nanotechnol.* **14**, 408 – 419 (2019).
- ⁶ Xiao Zhang, Yuelei Zhao, Qi Song, Shuang Jia, Jing Shi, and Wei Han, “Magnetic anisotropy of the single-crystalline ferromagnetic insulator $\text{Cr}_2\text{Ge}_2\text{Te}_6$,” *Jpn. J. Appl. Phys.* **55**, 033001 (2016).
- ⁷ G. T. Lin, H. L. Zhuang, X. Luo, B. J. Liu, F. C. Chen, J. Yan, Y. Sun, J. Zhou, W. J. Lu, P. Tong, Z. G. Sheng, Z. Qu, W. H. Song, X. B. Zhu, and Y. P. Sun, “Tricritical behavior of the two-dimensional intrinsically ferromagnetic semiconductor CrGeTe_3 ,” *Phys. Rev. B* **95**, 245212 (2017).
- ⁸ Yu Liu and C. Petrovic, “Critical behavior of quasi-two-dimensional semiconducting ferromagnet $\text{Cr}_2\text{Ge}_2\text{Te}_6$,” *Phys. Rev. B* **96**, 054406 (2017).
- ⁹ J. Zeisner, A. Alfonsov, S. Selter, S. Aswartham, M. P. Ghimire, M. Richter, J. van den Brink, B. Büchner, and V. Kataev, “Magnetic anisotropy and spin-polarized two-dimensional electron gas in the van der Waals ferromagnet $\text{Cr}_2\text{Ge}_2\text{Te}_6$,” *Phys. Rev. B* **99**, 165109 (2019).
- ¹⁰ Y. Sun, R. C. Xiao, G. T. Lin, R. R. Zhang, L. S. Ling, Z. W. Ma, X. Luo, W. J. Lu, Y. P. Sun, and Z. G. Sheng, “Effects of hydrostatic pressure on spin-lattice coupling in two-dimensional ferromagnetic $\text{Cr}_2\text{Ge}_2\text{Te}_6$,” *Appl. Phys. Lett.* **112**, 072409 (2018).
- ¹¹ Zhisheng Lin, Mark Lohmann, Zulfiqar A. Ali, Chi Tang, Junxue Li, Wenyu Xing, Jiangnan Zhong, Shuang Jia, Wei Han, Sinisa Coh, Ward Beyermann, and Jing Shi, “Pressure-induced spin reorientation transition in layered ferromagnetic insulator $\text{Cr}_2\text{Ge}_2\text{Te}_6$,” *Phys. Rev. Mater.* **2**, 051004 (2018).
- ¹² S. Selter, G. Bastien, A. U. B. Wolter, S. Aswartham, and B. Büchner, “Magnetic anisotropy and low-field magnetic phase diagram of the quasi-two-dimensional ferromagnet $\text{Cr}_2\text{Ge}_2\text{Te}_6$,” *Phys. Rev. B* **101**, 014440 (2020).
- ¹³ P. L. Alireza and G. G. Lonzarich, “Miniature anvil cell for high-pressure measurements in a commercial superconducting quantum interference device magnetometer,” *Rev. Sci. Instr.* **80**, 023906 (2009).
- ¹⁴ W. Schottenhamel, *Aufbau eines hochauflösenden Dilatometers und einer hydrostatischen SQUID-Druckzelle sowie Untersuchungen an korrelierten Übergangsmetalloxiden*, Ph.D. thesis, Technische Universität Dresden (2016).
- ¹⁵ B Bireckoven and J Wittig, “A diamond anvil cell for the investigation of superconductivity under pressures of up to 50 GPa: Pb as a low temperature manometer,” *J. Phys. E: Sci. Instrum.* **21**, 841–848 (1988).
- ¹⁶ G. Prando, R. Dally, W. Schottenhamel, Z. Guguchia, S.-H. Baek, R. Aeschlimann, A. U. B. Wolter, S. D. Wilson, B. Büchner, and M. J. Graf, “Influence of hydrostatic pressure on the bulk magnetic properties of $\text{Eu}_2\text{Ir}_2\text{O}_7$,” *Phys. Rev. B* **93**, 104422 (2016).
- ¹⁷ T. Sakurai, K. Fujimoto, R. Matsui, K. Kawasaki, S. Okubo, H. Ohta, K. Matsubayashi, Y. Uwatoko, and H. Tanaka, “Development of multi-frequency ESR system for high-pressure measurements up to 2.5 GPa,” *J. Magn. Reson.* **259**, 108 – 113 (2015).
- ¹⁸ The general pressure medium Daphne7373 ensures a hydrostatic pressure and gives good pressure homogeneity to the sample up to about 2.3 GPa. Therefore, it is sufficient for an FMR measurement with the maximum pressure of 2.4 GPa. The special pressure medium Daphne 7575 is necessary only for the magnetization measurement where a pressure above 3 GPa was applied in order to secure the pressure homogeneity in the high pressure range. See Refs. [19, 20] for details.
- ¹⁹ Keizo Murata, Keiichi Yokogawa, Harukazu Yoshino, Stefan Klotz, Pascal Munsch, Akinori Irizawa, Mototsugu Nishiyama, Kenzo Izuka, Takao Nanba, Tahei Okada, Yoshitaka Shiraga, and Shoji Aoyama, “Pressure transmitting medium Daphne 7474 solidifying at 3.7 GPa at room temperature,” *Rev. Sci. Instr.* **79**, 085101 (2008).
- ²⁰ Keizo Murata and Shinji Aoki, “Development of high pressure liquid medium with good hydrostatic pressure,” *Rev. High. Press. Sci. Tech.* **26**, 3–7 (2016), (*in Japanese with abstract in English*).
- ²¹ We did not use the other frequently applied method, the Arrot-plot technique [22], since it is not practicable for pressure dependent studies due to the reduced resolution stemming from the background signal of the pressure cell

- (see Sect. II).
- ²² I. Yeung, R. M. Roshko, and G. Williams, “Arrott-plot criterion for ferromagnetism in disordered systems,” *Phys. Rev. B* **34**, 3456–3457 (1986).
- ²³ J. A. Osborn, “Demagnetizing factors of the general ellipsoid,” *Phys. Rev.* **67**, 351–357 (1945).
- ²⁴ To minimize the undesired interference effects in the pressure cell and, in particular, to avoid the interference inside the sample we followed the recipe suggested in Ref. [25] and used very thin crystals with a thickness of a few tens μm which is much smaller than the shortest microwave wavelength of $1153\ \mu\text{m}$ at the highest applied frequency of 260 GHz. Furthermore, we repeated each experiment several times to confirm that the resonance fields agree within the error (less than the symbol size in Fig. 4(c)). This ensured that the intrinsic resonance position was always correctly obtained regardless the distortion.
- ²⁵ G Eilers, M von Ortenberg, and R Galazka, “Origin of Satellite Structures of High-Field EPR in $\text{Cd}_{1-x}\text{Mn}_x\text{Te}$,” *Int. J. Infrared Millimeter Waves* **15**, 695–722 (1994).
- ²⁶ D. C. Cronmeyer, “Demagnetization factors for general ellipsoids,” *J. Appl. Phys.* **70**, 2911 (1991).
- ²⁷ Stephen Blundell, *Magnetism in Condensed Matter* (Oxford University Press, Oxford, 2001).
- ²⁸ G. V. Skrotskii and L. V. Kurbatov, “Phenomenological theory of ferromagnetic resonance,” in *Ferromagnetic Resonance*, edited by S. V. Vonsovskii (Pergamon Press Ltd., 1966) Chap. Phenomenological Theory of Ferromagnetic Resonance, pp. 12–77.
- ²⁹ J. Smit and H. G. Beljers, “Ferromagnetic Resonance Absorption in $\text{BaFe}_{12}\text{O}_{19}$,” *Philips Res. Rep.* **10**, 113 (1955).
- ³⁰ Michael Farle, “Ferromagnetic resonance of ultrathin metallic layers,” *Rep. Prog. Phys.* **61**, 755 (1998).
- ³¹ Zhenhai Yu, Wei Xia, Kailang Xu, Ming Xu, Hongyuan Wang, Xia Wang, Na Yu, Zhiqiang Zou, Jinggeng Zhao, Lin Wang, Xiangshui Miao, and Yanfeng Guo, “Pressure-Induced Structural Phase Transition and a Special Amorphization Phase of Two-Dimensional Ferromagnetic Semiconductor $\text{Cr}_2\text{Ge}_2\text{Te}_6$,” *J. Phys. Chem. C* **123**, 13885–13891 (2019).
- ³² Kangying Wang, Tao Hu, Fanhao Jia, Guodong Zhao, Yuyu Liu, Igor V. Solovyev, Alexander P. Pyatakov, Anatoly K. Zvezdin, and Wei Ren, “Magnetic and electronic properties of $\text{Cr}_2\text{Ge}_2\text{Te}_6$ monolayer by strain and electric-field engineering,” *Applied Physics Letters* **114**, 092405 (2019).
- ³³ Riccardo Frisenda, Matthias Druempel, Robert Schmidt, Steffen Michaelis de Vasconcellos, David Perez de lara, Rudolf Bratschitsch, Michael Rohlfing, and Andres Castellanos-Gomez, “Biaxial strain tuning of the optical properties of single-layer transition metal dichalcogenides,” *Npj 2D Mater Appl* **1**, 10 (2017).